

Determining the Self-Limiting Electrospray Deposition Compositional Limits for Mechanically Tunable Polymer Composites

*Robert A. Green-Warren^{1,‡}, Luc Bontoux^{1,‡}, Noah M. McAllister¹, Dylan A. Kovacevich¹, Asaad
Shaikh¹, Christianna Kuznetsova¹, Max Tenorio¹, Lin Lei², Assimina A. Pelegri¹, Jonathan P.
Singer^{1,*}*

¹Department of Mechanical and Aerospace Engineering, Rutgers University, New Jersey 08854,
USA

²School of Materials Science and Engineering, Chongqing Jiaotong University, Chongqing
400074, China

ABSTRACT

Electrospray deposition (ESD) is a versatile micro/nano coating technology that utilizes the competition between surface charge of a droplet and its surface tension to create monodisperse generations of micro/nano droplets. ESD can deposit uniform thin films by including dilute solutes in these droplets. One mode of ESD, self-limiting electrospray deposition (SLED), has been shown to exist when glassy polymers are sprayed in a volatile solvent below the polymer glass transition temperature (T_g). This leads to charge accumulation on the coating surface that slows the growth of the film thickness. Since solutes can be easily blended in dilute ESD solutions, we investigate the SLED limits of self-limiting and non-self-limiting solute blends. As a motivating application, we focus on mechanical properties of the film. Specifically, we blend self-limiting polystyrene (PS) and SU-8 epoxy resin with different non-self-limiting mechanical modifiers, such as plasticizers and curing agents. To characterize the resulting morphologies and mechanical properties, we employ scanning electron microscopy and nanoindentation of as received and smoothed films. The results illustrate the formation of composited polymers that exhibit self-limiting ability by SLED, depending on the interaction between the two components. Further, mechanical properties could be effectively fine-tuned within these compositional ranges. This signifies the 3D coating capabilities through SLED can be implemented incorporating additional functionalities and properties beyond the base matrix.

KEYWORDS

Electrospray deposition, Polymers, Composites, Nanoindentation, Coatings

INTRODUCTION

Polymer thin films are being studied at an accelerating rate due to their application in modern engineering systems. Such applications include selective membranes for microfiltration systems, hydrophobic barriers for microelectronic devices, encapsulation of micro/nano-scale biomedical devices, and separation membranes for energy storage systems. Many studies have considered nanoscale coatings produced conventionally by vapor deposition or electrodeposition. However, these methods require a fluid bath during the coating process or vacuum-based machinery and only work with a narrow selection of coating material^{1,2}. For more flexible brush, dip, and blade coating approaches, poor coating process control leads to non-uniform coverage on both 2D and 3D targets due to capillary effects³⁻⁵.

Electrospray deposition (ESD) has been developed for micro/nano scale coatings in the past few decades⁶⁻¹⁴ to reduce material waste and increase coating uniformity. ESD utilizes the competition between electrostatic force and surface tension of the solution to form a Taylor cone at the tip of a charged nozzle. Then, atomization of the solution produces microscale droplets when the voltage reaches a critical value. As the solvent evaporates during descension, the charged droplet reaches the Rayleigh limit and then transitions into monodispersed child droplets. This transition is followed by repeated Coulomb fission events as the droplets approach the spraying target¹⁵. The diameter of a majority of the droplets produced in ESD from the Taylor cone jet has been correlated with the fluid properties and spray flow rate as¹⁶:

$$d = \alpha \left(\frac{Q^3 \epsilon_0 \rho}{\pi^4 \sigma \gamma} \right)^{\frac{1}{6}} + d_o \quad (1)$$

where α is a constant related to the fluid's dielectric permittivity, ρ is the density, γ is the surface tension, σ is the electrical conductivity, Q is the flow rate, ϵ_0 is the permittivity of free space and d_o is a small droplet diameter only significant at low flow rates.

Control of these parameters illustrate the advantages of this ESD over conventional coating techniques including: (1) the generation of monodisperse droplets resulting in uniform deposition; (2) the final droplet size, which can be down to hundreds of nanometers, thereby highlighting ESD as an effective method for micro/nanoscale coatings; (3) Morphologies of thin films can be readily modified by adjusting the spray conditions, such as flow rate; (4) The spray is efficiently delivered directly to the target without overcoat; (5) The spray processing can be accomplished in an ambient environment and at atmospheric pressure¹⁷.

An extension of ESD, coined self-limiting electrospray deposition (SLED) has been demonstrated by only spraying glassy insulating materials below their glass transition temperature (T_g) and mixed with a volatile solvent onto a sufficiently conducting substrate¹⁸⁻²². A limited thickness will be achieved as charges accumulate with increased spray time and spray is redirected to uncoated parts of the target. We have employed different polymers to investigate the mechanism of self-limiting through ESD. The results indicate that the critical thickness of SLED is determined by the total mass of sprayed polymer solids, the strength of electric field, and the composition (*e.g.*, dielectric strength, distance from T_g , solvent affinity) of the spray solvent and polymer. Each of these parameters significantly impacts the thickness and morphology of thin films produced by SLED. For example, SLED coatings produced by in-air gelation of methylcellulose delivers

nanowire SLED coatings as opposed to the rounded morphologies more frequently observed²². Notably, SLED allows for uniform coatings on complex 3D structures as a post-processing treatment¹⁸, including 3D printed microlattices²³ and natural structures²².

Depositing blends through ESD is straightforward due to the ease of mixing dilute solutes. For example, the degree of crystallinity of the semiconducting polymer films prepared by ESD can be enhanced through modifying blending ratios²⁴⁻²⁶. In Hao et al.'s study, ESD was additionally employed to manufacture porous particles by blending drug and biodegradable polymers to precisely control the release rate of a drug⁸. Other than blending soluble polymers, solids have also been widely added into precursor solutions for spray. We have previously demonstrated that functional nanowires with tunable optical properties can be produced by spraying the composites of plasmonic nanoparticles and that they became better dispersed with the addition of a plasticizer²⁷. In fabricating fuel cell electrodes, the spray of blended catalyst particles and electrolytic solutions led to 3D nanostructures with large porosity and high surface area, enhancing the device performance^{7, 28, 29}. Most relevant for the current investigation, we employed PS and styrenic block copolymers in a blended solution to change the surface properties of a 3D printed hydrogel lattice¹⁹. The hydrogel coatings revealed that the non-self-limiting material blended with a self-limiting component maintains the ability to achieve uniform coatings on 3D complex structures. Additionally, swelling tests in this work demonstrated that the coating's mechanical properties, due to the plasticizing copolymer, were compliant enough to resist changes in lattice size by up to 16%. This example illustrates both that there exists a compositional limit of non-self-limiting and self-limiting blends to be still compatible with SLED and that there are functional benefits to exploring these blends.

Here we investigate the SLED compositional limits of polymer blends through ESD. In this study, all samples were prepared by spraying composites with self-limiting and non-self-limiting components with various blend ratios. The immiscible blends include: PS 35 kDa:Kraton D1102 (Kraton) and SU-8:Soy oil. PS, a thermoplastic polymer with $T_g \sim 100$ °C, has been chosen as a model material with 2-butanone for obtaining SLED 3D coating in our previous work¹⁸. Kraton is a linear styrene-butadiene-styrene (SBS) tri-block copolymer (BCP) with ~ 70 wt% butadiene ($T_g \sim -100$ °C) that is non-self-limiting and leads to the BCP being non-self-limiting, as we have previously shown.³⁰ Mechanically, Kraton can be used as a plasticizer for PS. SU-8 is an oligomeric epoxy resin that has a $T_g \sim 60$ °C. Oils are regularly used as resin plasticizers. Miscible composites include: PS 850 Da:PS 35 kDa and SU-8:Versamid 125 (Versamid). Versamid is a reactive amide crosslinking agent that reacts with the epoxide groups in the SU-8 oligomer. Transitions to self-limiting behavior were identified by evaluating changes in the central thickness after thermal smoothing of the film and visible appearance of the coatings. Porous and condensed samples prepared by SLED method were examined by nanoindenter tests to evaluate the mechanical properties of select composites.

EXPERIMENTAL SECTION

PS (molecular weight (MW)=35 kDa and 850 Da, Sigma Aldrich), Kraton D1102 (PolyOne GLS), SU-8 (EPON Resin SU-8), and soybean oil (Sigma Aldrich) were used as received from the manufacturer. Versamid 125, a reactive polyamide resin, was used as curing agent to make SU-8 composites. 2-butanone (>99%, Sigma Aldrich) was used as received as the carrier solvent for the spray solutions.

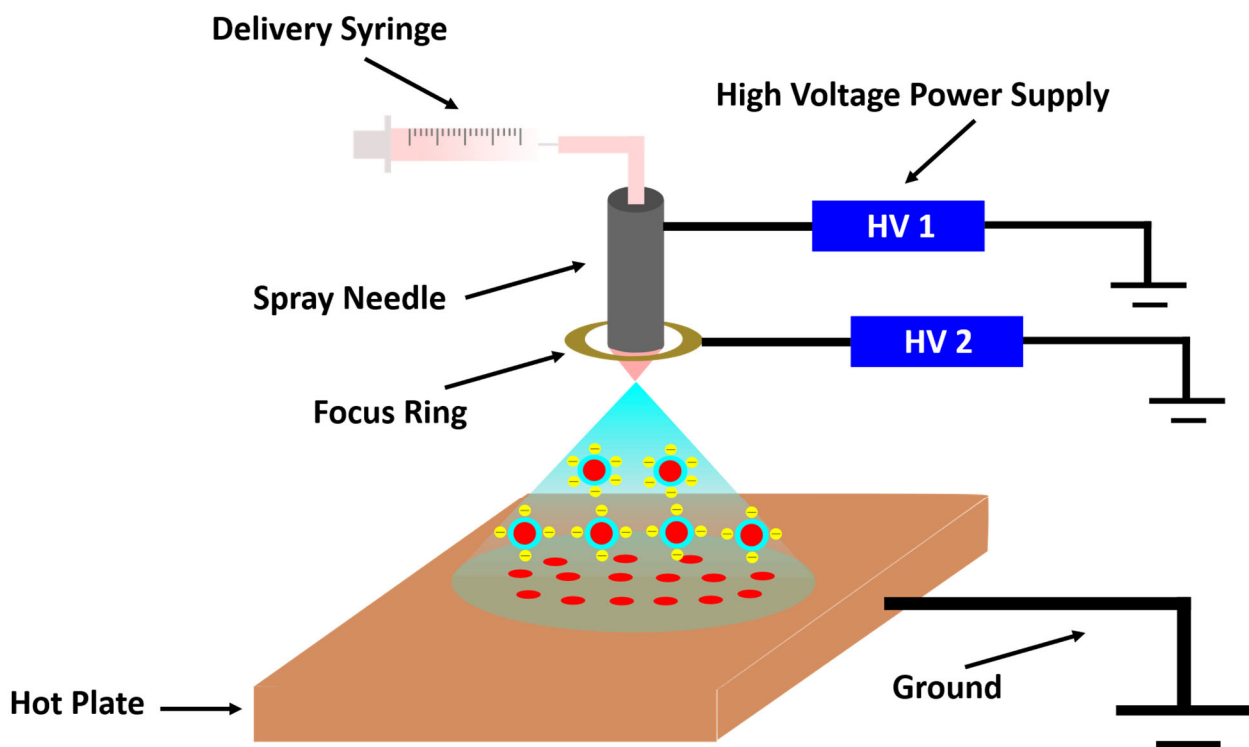


Figure 1. Schematic diagram of electro spray deposition setup.

The schematic image of electro spray deposition shows in Figure 1. The setup includes four main parts: (1) a syringe pump (KD Scientific), a stainless needle (Sai Infusion, 20 gauge, 1.5”) and (2) a steel focused ring (inner diameter of 2 cm and an outer diameter of 4 cm) with (3) two negative high-voltage power supplies (Acopian), (4) a 10 cm circular collection silicon wafer (University Wafer), placed in the center of the hotplate. The wafer was secured with an alligator clip attached to the ground wire during spray. Samples for nanoindentation tests were obtained by spraying 2.5 cm × 1 cm rectangular silicon chips.

Silicon wafers and chips were cleaned and degreased by acetone and ethanol before spray. All of the precursor solutions for blends spray were made at 1 wt%, and mixed in different ratios: 0:1,

1:5, 1:2, 1:1, 2:1, 5:1, 1:0. Samples were sprayed for 60 minutes while setting the spray target distance to 4 cm, with flow rate of 0.5 mL/hr. The PS 35 kDa:PS 850 Da and PS 35 kDa:Kraton blends were sprayed at 35 °C to be more consistent with past results, and the SU-8:Versamid, SU-8:Soy oil, and SU-8:PS 35 kDa blends were sprayed at room temperature (~20 °C) to not approach the T_g of SU-8. The driving voltage was set to approximately -5.4 kV. The stability of the Taylor cone was prioritized during spray: in sprays that were unstable at the nominal driving voltage (-5.4 kV), the driving voltage was set between -5.0 kV and -5.8 kV. The focus ring was set ~ 1 cm above the needle tip and the voltage was maintained between -2.7 kV and -3.3 kV. The Taylor-cone jet spray was utilized for all experiments in this study. The humidity was monitored and fell between 20% - 60% for each spray. Condensed PS and Kraton composite films were made by post thermal treatment at 120 °C for ~10 s. To smooth SU-8:Versamid films for measuring thickness, samples were heated between 80 ~ 100 °C for ~10 s. The remainder of the crosslinking, as with the porous sample, was allowed to occur at room temperature. The experimental conditions for all samples can be found in Table S1.

A microscopic reflectometer (Filmetrics F40) and a motorized stage (Zaber E13F33E) were used to measure film thickness. To examine the self-limiting regime of samples, a linear mapping profile was collected using 200 points in a line, which covered the full range of the deposited film. The central 1 cm region of the profile was for calculating central thickness. The thickness of the chip samples for indentation tests was measured by mapping 100 points in a 10 x 10 square with 1 mm distance in the central 1 cm² of the film. For select samples, 45° cross-sectional imaging using a Zeiss Sigma field emission scanning electron microscope (SEM) was employed to characterize the spray morphology.

The mechanical properties, including hardness (H) and reduced modulus (E_r) of different polymer composites, were tested by using nanoindentation (Hysitron TI750 Ubi and NanoTest Vantage). The data obtained were analyzed by the native software packages included with the nanoindentation systems. This study utilized two nanoindenter tips: a Berkovich tip, defined as a 3-sided pyramid with included angles of 65.3° from the vertical, and a conospherical tip with a radius of $10\ \mu\text{m}$, for the Hysitron and Vantage, respectively. Indentations on the porous films were conducted on the Vantage with the conospherical tip to mitigate the effects of surface roughness and contact angle. The Hysitron was used to perform indents on the dense samples utilizing the Berkovich tip to minimize the indentation depth.

To measure the mechanical properties via nanoindentation, a load-controlled experiment was employed. In this regime, the nanoindenter goes into the material to a maximum specified load and the corresponding indentation depth is recorded. To avoid the artifacts associated with film-substrate interactions, single indent depth-controlled experiments were initially performed to determine the maximum load at which $\sim 10\%$ of the film thickness was achieved during this indentation cycle. The load corresponding to this 10% depth was then prescribed as a maximum load during the actual experiment. A 5-2-5 load function with varying peak loads was used while keeping segment times constant. This load function represents a five-second loading time, a two-second hold time at the maximum load, and a five second unload time. For the unsmoothed samples, a 10×10 indentation grid with a constant $0.1\ \text{mN}$ load was implemented, for a total of 100 indents each spaced $30\ \mu\text{m}$ apart. Whereas, for the smoothed samples five 5×5 indentation grids, totaling 125 indents, were conducted at select locations on the film, with a grid spacing of

60 μm . Three of the five grids were completed with a constant load function, while the remaining two grids varied the load from 400 μN to 0 μN . This was done to ensure that the results were consistent across a range of depths. Three compositions, namely, pure PS 35 kDa, PS 35 kDa:Kraton (1:1), and SU-8:Versamid (2:1), were selected for nanoindentation testing. For each blend, both a porous and a dense sample was indented, leading a total of six samples on which mechanical analysis was performed. Crosslinked samples were allowed to cure at room temperature for at least 24 hours prior to measurement.

RESULTS

Our previous study demonstrated that 1 wt% diluted PS in 2-butanone sprayed at a flow rate of 0.5 mL/hr and a substrate temperature of 35 °C at a distance of 4 cm was a condition, among others, that reliably displayed self-limiting results. These spray conditions were used as the defaults to implement homogeneous and blended samples in this study; however, samples that contained SU-8 were sprayed at room temperature since SU-8's glass transition temperature is much lower than PS. The coating thickness of the blends was compared with the standard thickness-limited PS and SU-8 films in order to evaluate the self-limiting ability of the different blends. Figure 2 depicts the selected miscible and immiscible blends along with the central thickness of post-smoothed films plotted against the volume fraction of each substance. Photographs of pure materials sprays and select transition-state samples can be found in Figure S1. Figure 2a-b shows that two miscible components deposited as blends. In Figure 2a, as the self-limiting PS 35 kDa was gradually added to non-self-limiting, charged melt PS 850 Da, the film thickness varies linearly from pure PS 850 Da of $4.3 \pm 0.3 \mu\text{m}$ to the SLED thickness of pure PS 35 kDa in these conditions ($2.6 \pm 0.4 \mu\text{m}$).

SU-8:Versamid composites in Figure 2b demonstrates a transition from a plateau near the electrowetted thickness ($3.1 \pm 0.1 \mu\text{m}$) of pure Versamid to the pure SU-8 SLED thickness of $2.6 \pm 0.3 \mu\text{m}$.

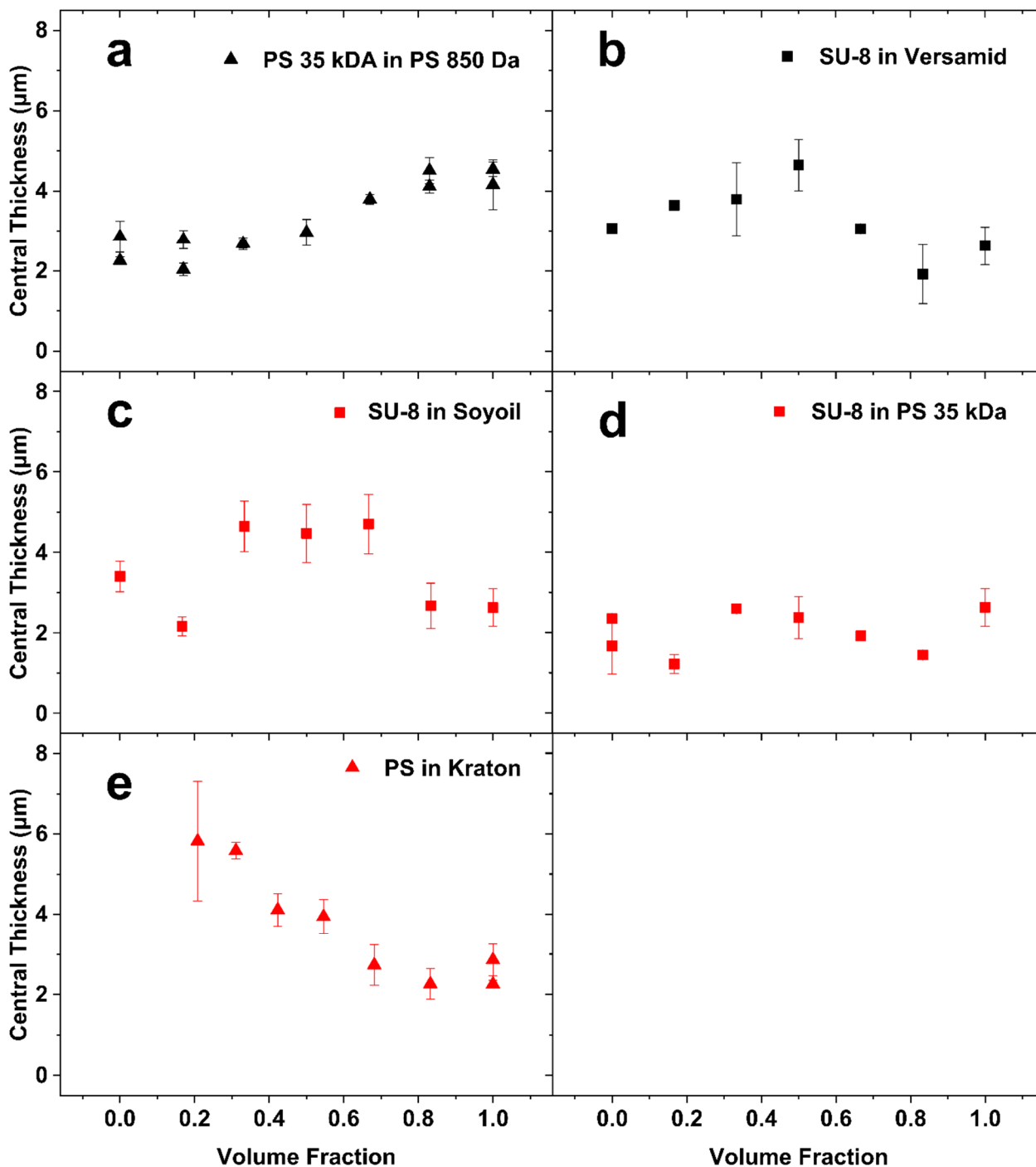


Figure 2. (a-b) Miscible blends sprayed at different volume fractions: (a) PS 850 Da:PS 35 kDa, (b) SU-8:Versamid. (c-e) Immiscible blends sprayed at different volume fractions: (c) SU-8:Soy oil, (d) SU-8:PS 35 kDa, (e) PS 35 kDa:Kraton. In (e) the reported volume fraction considers the PS content in the Kraton SBS BCP. All blends were sprayed at 1 wt% solids, at 0.5 mL/hr for 60 min; (a,e) were sprayed at 35 °C, and (b-d) were sprayed at room temperature (~20 °C). Each data point represents the result of a single spray. The sixth panel is deliberately blank.

For the spray of immiscible polymer blends in Figure 2c-e, the tendency of thickness variation becomes more complex than miscible blends. As Figure 2c illustrates, the thickness of pure sprayed soy oil transitions from electrowetting with low-thickness of $3.3 \pm 0.3 \mu\text{m}$ to a rough charged melt regime (with a maximum average thickness at 0.167 volume fraction of $6.1 \pm 0.3 \mu\text{m}$) before reaching the self-limiting thickness of pure SU-8. In Figure 2d, the composites of PS 35 kDa and SU-8 maintain the ability to be thickness-limited when the ratios are adjusted with a non-monotonic change in central thickness. The central thickness of deposited blends was similar to the self-limiting thickness of PS 35 kDa ($\sim 2 \mu\text{m}$) with a subtle minimum when the fraction of SU-8 was lower than $\sim 60 \text{ vol}\%$. When the fraction of SU-8 increased above 60 vol%, the thickness limit gradually approached the self-limiting thickness of pure SU-8. In Figure 2e, the central thickness of Kraton is $5.8 \pm 1.4 \mu\text{m}$ with large roughness typical of what we call a “charged melt” spray (Figure S1c). This regime is characterized by cellular electrostatic instabilities (“Taylor-Bénard cells”¹⁸) and has the smallest spot size of the insulating sprays measured here. With the addition of PS 35 kDa, the film thickness decreases in an apparent stepwise fashion again, showing either a plateau or minimum before reaching the SLED thickness of PS.

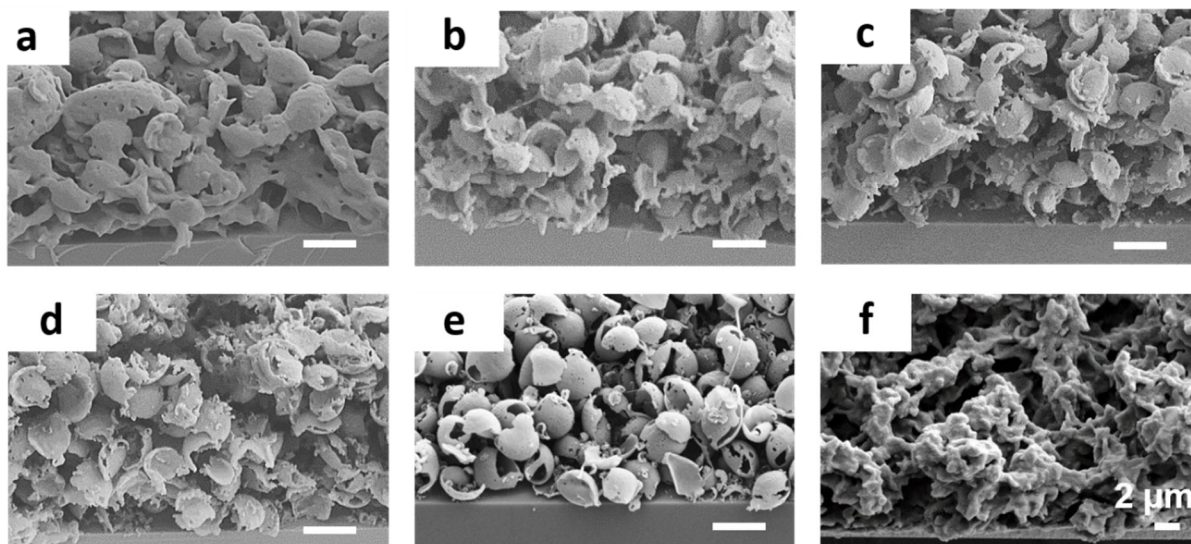


Figure 3. Cross-sectional SEM images of 1 wt% total solids of PS 35 kDa:Kraton and SU-8:Versamid of different ratios sprayed at 0.5 mL/hr for 60 min at 35 °C. (a) 1:2 (PS 35 kDa:Kraton); (b) 1:1 (PS 35 kDa:Kraton); (c) 2:1 (PS 35 kDa:Kraton); (d) 5:1 (PS 35 kDa:Kraton); (e) 1:0 (PS 35 kDa:Kraton); (f) 2:1 (SU-8:Versamid).

To demonstrate the change in microscale morphology, cross-sectional SEM was used. Figure 3a-f are SEM images of 1 wt% PS 35 kDa with Kraton blend samples sprayed in different ratios. In Figure 3a, since the spray temperature is much higher than the T_g of the butadiene block of the BCP and there is only 36 wt% of the styrene fraction for sprayed droplets, the miscible blend forms a continuous porous film with only few hollow-shell structures on the surface. However, when the concentration of PS increased, the morphology of PS:Kraton composites varied from connected discs to more integrated spherical shells in Figure 3b-e. For the SU-8:Versamid blend, the crosslinking agent similarly plasticizes and fuses the deposited particles. The porous structure in Figure 3f indicates that the blends spray of SU-8:Versamid leads to a crosslinked porous network

via ESD. Based on our observations, the fusing in the SU-8:Versamid films is a gradual process that continues after spray, with 1:1 ratios spraying as powder films before auto-leveling into optically dense films during the gradual crosslinking (**Figure 4**).

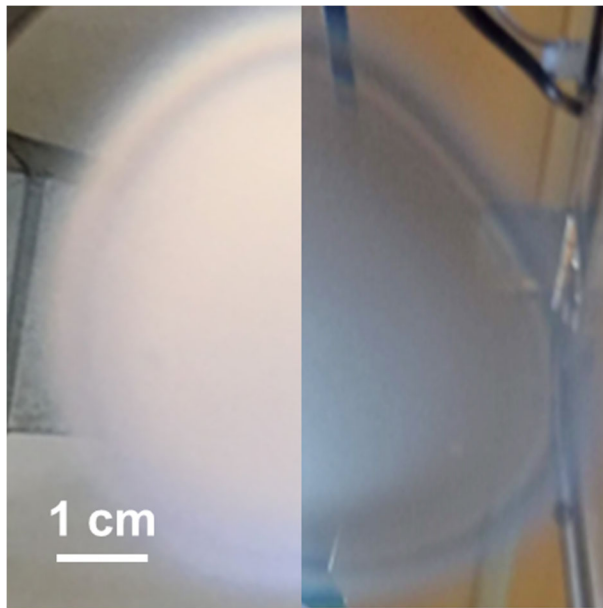


Figure 4. Photographs of an SU-8:Versamid 1:2 blend coating before (left) and after (right) 1 day of auto-leveling at room temperature.

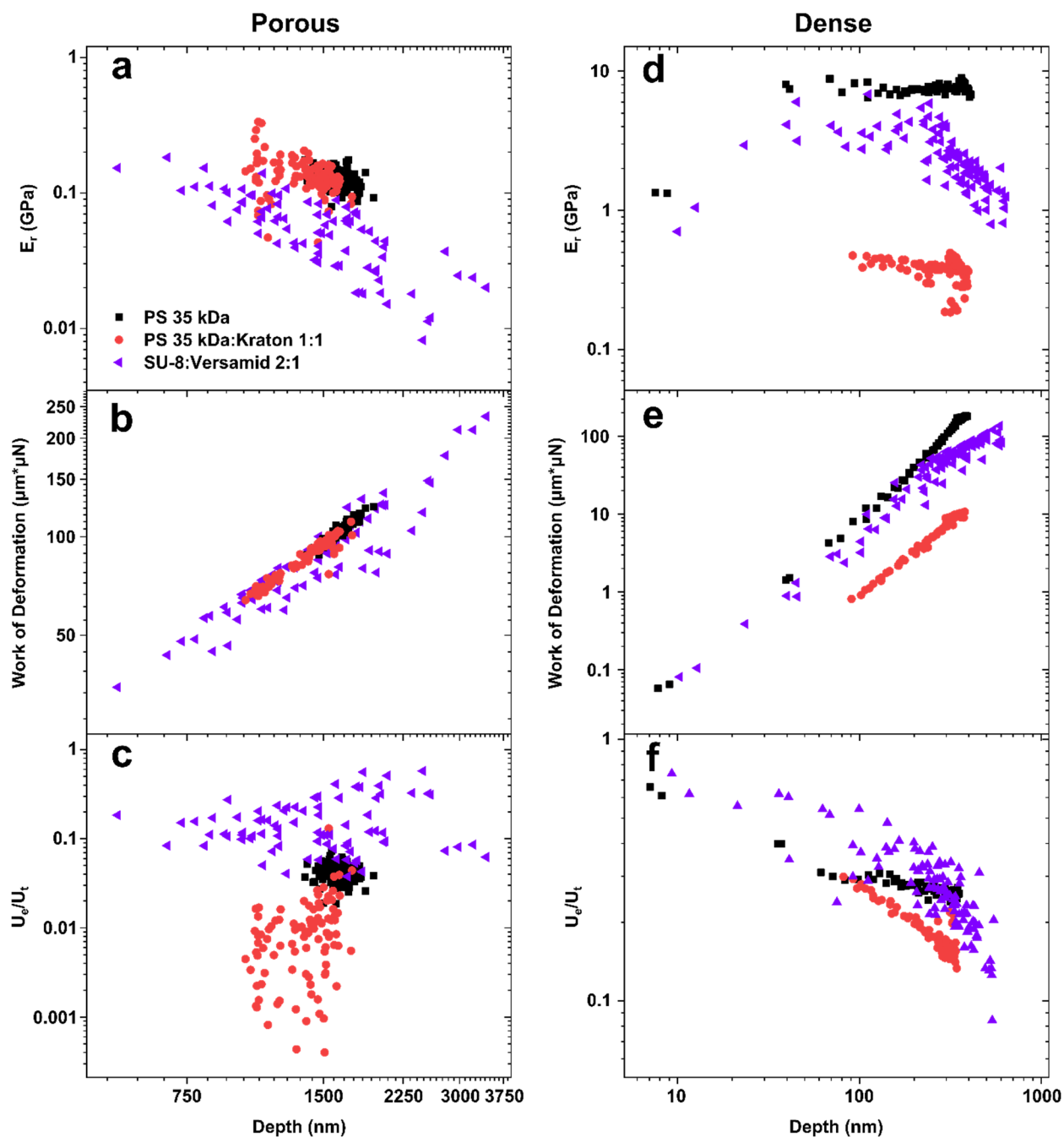


Figure 5. Nanoindentation results of porous (a-c) and condensed (d-f) blends created by ESD: (a, d) reduced modulus vs depth; (b, e) work of deformation vs depth; (c, f) ratio of elastic potential to total potential vs depth.

Figure 5a-d shows the nanoindentation results of both porous and condensed sprayed thin films. Figure 5a shows that the reduced modulus, E_r , of porous films decreases as the indentation depth varies from 200 nm to 3750 nm. With the indent depth increasing, the reduced modulus of porous SU-8:Versamid changes from ~ 0.1 GPa to ~ 0.01 GPa, and the value tends to be less than both the PS 35 kDa and PS 35 kDa:Kraton samples for comparable depth. At early indents, the smoothed SU-8:Versamid has a reduced modulus of 4.0 ± 1.3 GPa before reducing rapidly at higher loadings. Porous pure PS 35 kDa and PS 35 kDa:Kraton have similar moduli ~ 0.01 GPa, corresponding to each indentation depth. In Figure 5d, smoothed pure PS 35 kDa thin film exhibited the highest reduced modulus of nearly 7.8 ± 0.4 GPa, which, while higher than may be expected for bulk PS, is similar to other confined PS films measured by indentation.³¹ The smoothed PS 35 kDa:Kraton blend shows the lowest reduced modulus around 0.43 ± 0.05 GPa. Figure 5b and e show the work done during nanoindentation tests. Figure 5b indicates that the SU-8:Versamid sample necessitates the most work to reach the indent depth of 1000 nm. Additionally, Figure 5b illustrates that the PS 35 kDa and PS 35 kDa:Kraton samples require similar amount of work deformation for identical depths of indentation. Values of work on different samples seemed to increase linearly with indentation depth on a log-log scale. For condensed samples, the nanoindenter does the most work on the pure PS 35 kDa sample when compared to both SU-8:Versamid and PS 35 kDa:Kraton samples as illustrated in Figure 5e.

DISCUSSION

While we have identified categories of ESD of glassy materials based on viscosity and charge dissipation, it is important to note that, for the most part, these classifications are continua. For example, in the case of the transition from electrowetting sprays to charged melt sprays, the

balance of charge injection/dissipation and coating mobility determines whether it is more efficient to dissipate charge via electrostatic instability or wetting. This switch can even occur during the spray as the thickness of the coating makes it too difficult to dissipate charge through wetting. Such an example is PS 850 Da, which clearly displays both highly smooth and high roughness regions at the edge and center of the spray respectively (Figure S1f) Whereas for the transition between self-limiting and a charged melt evinces a powder becomes increasingly densified during the parameter change until it is better described as a viscous liquid. Optically, this can be observed as a reduction in scatter, as in SU-8:Versamid 1:1 (Figure 4, Figure S1h). For miscible composites, adding self-limiting component initiates this transformation gradually, with the visible transition to a powder coating appearing with less than 20 vol% self-limiting components added. This is similar to what was observed when increasing temperature in our previous work.¹⁸ SEM results also confirm this transition through surface morphology changes to a fused shell assembly (Figure 3). The higher conductivity and solvent interaction of the polymer network with the polymer approaching its T_g allowed for enhanced charge dissipation. In other words, the mechanism of phenomenological changes in miscible blends spray is attributed to the added self-limiting components (PS 35 kDa, SU-8) increasing T_g of blends. The pure self-limiting species also display different behaviors. The pure PS spray is more stable but thicker than the pure SU-8. Both of these effects are consistent with our past results with SU-8 possessing higher dielectric constant, but more facile solvent swelling and low glass transition due to the oligomeric nature of the substance.²⁰ It is interesting to note that the addition of either miscible or immiscible components does appear to stabilize the thickness of the SU-8, which is suggestive that additives offset this sensitivity to solvent.

For immiscible blends, adding solid self-limiting components into liquid non-self-limiting materials displays more complex effects (Figure 2c, d). In the spray of SU-8:Soy oil, the low viscosity soybean oil goes from a near-electrowetting state to a thick charged melt due to the addition of immobile glassy domains. After stabilizing at a charged melt thickness of $\sim 5 \mu\text{m}$ for a wide compositional range, the blend becomes more self-limiting and takes on a powdery appearance as the oil becomes dispersed in the SU-8. In contrast, the composites of the two self-limiting components (Figure 2e) always lead to a self-limiting spray with a subtle local minimum in thickness observed when PS 35 kDa is first added to SU-8. We have previously observed that, while SU-8 is sensitive to solvent, its higher dielectric strength leads to it being more self-limiting as a mask material.²⁰ Taken together with the fact that blending seems to stabilize SU-8 sprays to solvent effects, it follows that adding PS to SU-8 would improve the stability.

The BCP results echo many of these trends but in a stepwise fashion. The microphase separation that occurs within a BCP with strongly immiscible blocks results in thermodynamically-determined ordered phases,³² and can be considered a confined version of the immiscible blend effects. In the pure Kraton case having high butadiene fraction ($T_g \sim -100 \text{ }^\circ\text{C}$), a thick charged melt was observed due to the viscous enhancement of the glassy PS inclusions, which at the starting fraction should be a combination of at the starting fraction micelles and partially-formed cylinders. Adding PS to this mixture is expected to initially swell the PS domains, having little effect on the overall morphology.³³ Then, as the fractions approach one another, there is a step down in thickness that aligns with the nominal transition to lamellar morphology. Here, the low- T_g material and high- T_g are both continuous phases, leading to a self-limiting immobile state that is a relatively poor self-limiting material similar to pure SU-8. This can be seen in the morphology as a fused

network of shells (Figure 3a). Increasing the amount of PS further results in a final step in thickness. The morphology most likely transitions to swollen BCP domains contained in a matrix of excess PS as the ability to expand the domains fails in favor of macrophase separation.³³ This breaks the continuity of the low- T_g phase, seen in the SEM as gradual definition being added to the shell network (Figure 3c-e) approaching the morphology of pure PS (Figure 3f). There may additionally be a small local minimum with the 5:1 PS 35 kDa:Kraton composition similar to the PS 35 kDa:SU-8 blends, but it is below the error threshold. However, this would likely correspond to a morphology of BCP micelles with a polybutadiene core in the PS matrix.

We evaluated the ability to tune mechanical properties of the composites by employing nanomechanical measurements. In the porous state, the reduced moduli of the PS and plasticized PS 35 kDa:Kraton composite are similar, while the SU-8-Versamid is lower and shows scatter associated with brittle failure. Once densified, the PS 35 kDa:Kraton becomes much less stiff relative to PS and the crosslinked epoxy also becomes less stiff, revealing the effects of the collapsed and fused porous structure caused by the compositing. While the plasticized composite is much softer than the PS, the porous form is more fused and collapsed, leading to a relatively higher apparent reduced modulus. All samples displayed power-law plastic energy deformation, shown in Figure 5b,e.

	Material	Exponent	R²
	PS 35 kDa	1.03	0.90

Porous	PS 35 kDa:Kraton 1:1	0.96	0.93
	SU-8:Versamid 2:1	0.92	0.87
Dense	PS 35 kDa	2.18	0.99
	PS 35 kDa:Kraton 1:1	1.96	0.96
	SU-8:Versamid 2:1	1.85	0.80

Table 1. Power equations and R^2 values for each of the materials in both porous and densified states.

Table 1 tabulates the power law exponent equations fitted to the work of deformation plots for each material. Each of the equation fits has R^2 values above, with pure PS achieving the best fit. The densification process increases the exponent, the degree of strain hardening, in each case by roughly a factor of 2. PS has the highest exponent due to its relative ability to resist indentation as a rigid, plastically deformable material, which is reduced by plasticization. In each sample, a dramatic increase in the stiffness can be seen after the sample has been densified. This is illustrated in Figure 5 when comparing plots b and e. The densified samples require nearly an order of magnitude more work to achieve indents of the same depth. This demonstrates the ability of the materials to dissipate energy in their porous state and store energy in their condensed state. The variation in the reduced modulus of the SU-8:Versamid 2:1 specimen points to apparent spatial variation in the stiffness across the surface of the sample, which is most likely due to the creation of brittle fractures in the crosslinked system. These cracks relieve stress and result in lower apparent reduced modulus but do not always occur, resulting in the scatter. This also prevents plastic deformation, leading to the lowest overall exponent.

Previously, the ratio of elastic indentation work to total indentation work has been employed to characterize the degree of energy dissipation of silicone rubber thin films.³⁴ Therefore, the lack of plasticity associated with the smoothed SU-8:Versamid is also illustrated in Figures 5c,f. The SU-8:Versamid 2:1 demonstrates the most elastic recovery of the three materials both before and after densifying. The high values of work of deformation for the SU-8:Versamid 2:1 can be explained by Figure 5c,f. The increased load needed to perform an indent causes the deformation work to be higher for an equally deep indent. This comparatively high load required for an indent of equal depth in SU-8:Versamid 2:1 is also reflected in its reduced modulus values.

CONCLUSIONS

We have established the capability to create self-limiting micro coatings through ESD of glassy polymers blended with non-glassy modifiers and the compositional limits of this blending to maintain the SLED effect. The results show that non-self-limiting modifiers of up to 40 vol.% can be added without disrupting the self-limiting behavior. Further, these modifiers can alter the mechanical properties. This presents the ability to tune the characteristic mechanical behavior (*i.e.*, brittle, elastic, plastic) and the observed contact response through the blending approach. By selecting composition, the mechanism of the mechanical response can be tuned, while the degree of densification, which can be controlled thermally through partial densification, can set the contact mechanics. Since these blends maintain the SLED effect, functional coating of 3D objects with selected mechanical properties can be manufactured for various applications. In the future, we additional functional modifiers can be pursued, such as spatially-selective crosslinking, tunable

surface adhesion, as well as non-mechanical effects such as electrical or thermal conductivity, chemical activity, or optical modification.

ASSOCIATED CONTENT

Supporting Information

The following files are available free of charge.

brief description (file type, i.e., PDF)

AUTHOR INFORMATION

Corresponding Author

*Email: Jonathan.singer@rutgers.edu

ORCID

Jonathan P. Singer: 0000-0002-5934-8795

Author Contributions

R.A.G.-W. and L.B. contributed equally to this work. The manuscript was written through contributions of all authors. All authors have approved the final version of the manuscript.

Funding Sources

This work was partially funded by the NSF through CMMI Award 2019849. J.P.S. acknowledges the 3M Company through the 3M Non-Tenured Faculty Award. R.A.G.-W. acknowledges the National GEM Consortium. L.B., D.A.K., and C.K. acknowledge the New Jersey Space Grant Consortium, funded by NASA, through their student fellow program.

REFERENCES

1. Jung, Y. C.; Bhushan, B., Mechanically durable carbon nanotube– composite hierarchical structures with superhydrophobicity, self-cleaning, and low-drag. *ACS nano* **2009**, *3* (12), 4155-4163.
2. Zhang, Y.; Zhang, L.; Zhou, C., Review of chemical vapor deposition of graphene and related applications. *Accounts of chemical research* **2013**, *46* (10), 2329-2339.
3. Brinker, C.; Frye, G.; Hurd, A.; Ashley, C., Fundamentals of sol-gel dip coating. *Thin solid films* **1991**, *201* (1), 97-108.
4. Nguyen, D. D.; Tai, N.-H.; Lee, S.-B.; Kuo, W.-S., Superhydrophobic and superoleophilic properties of graphene-based sponges fabricated using a facile dip coating method. *Energy & environmental science* **2012**, *5* (7), 7908-7912.
5. Pierre, A.; Sadeghi, M.; Payne, M.; Facchetti, A.; Anthony, J.; Arias, A., All-printed flexible organic transistors enabled by surface tension-guided blade coating. *Advanced materials (Deerfield Beach, Fla.)* **2014**, *26* (32), 5722.
6. Morozov, V. N.; Morozova, T. Y., Electrospray deposition as a method to fabricate functionally active protein films. *Analytical chemistry* **1999**, *71* (7), 1415-1420.
7. Martin, S.; Garcia-Ybarra, P.; Castillo, J., Electrospray deposition of catalyst layers with ultra-low Pt loadings for PEM fuel cells cathodes. *Journal of Power Sources* **2010**, *195* (9), 2443-2449.
8. Hao, S.; Wang, Y.; Wang, B.; Deng, J.; Zhu, L.; Cao, Y., Formulation of porous poly (lactic-co-glycolic acid) microparticles by electrospray deposition method for controlled drug release. *Materials Science and Engineering: C* **2014**, *39*, 113-119.
9. Xie, J.; Tan, J. C.; Wang, C.-H., Biodegradable films developed by electrospray deposition for sustained drug delivery. *Journal of pharmaceutical sciences* **2008**, *97* (8), 3109-3122.
10. Hu, H.; Singer, J. P.; Osuji, C. O., Morphology development in thin films of a lamellar block copolymer deposited by electrospray. *Macromolecules* **2014**, *47* (16), 5703-5710.
11. Hu, H.; Rangou, S.; Kim, M.; Gopalan, P.; Filiz, V.; Avgeropoulos, A.; Osuji, C. O., Continuous equilibrated growth of ordered block copolymer thin films by electrospray deposition. *ACS nano* **2013**, *7* (4), 2960-2970.
12. Kim, J. W.; Yamagata, Y.; Kim, B. J.; Higuchi, T., Direct and dry micro-patterning of nano-particles by electrospray deposition through a micro-stencil mask. *Journal of Micromechanics and Microengineering* **2009**, *19* (2).
13. Steipel, R. T.; Gallovic, M. D.; Batty, C. J.; Bachelder, E. M.; Ainslie, K. M., Electrospray for generation of drug delivery and vaccine particles applied in vitro and in vivo. *Materials Science and Engineering: C* **2019**, *105*, 110070.
14. Shlyapnikov, Y. M.; Shlyapnikova, E. A.; Morozov, V. N., Reversible and Irreversible Mechanical Damaging of Large Double-Stranded DNA upon Electrospraying. *Anal Chem* **2016**, *88* (14), 7295-301.
15. Jaworek, A.; Sobczyk, A. T., Electrospraying route to nanotechnology: an overview. *Journal of Electrostatics* **2008**, *66* (3-4), 197-219.
16. Gañán-Calvo, A. M.; Dávila, J.; Barrero, A., Current and droplet size in the electrospraying of liquids. Scaling laws. *Journal of Aerosol Science* **1997**, *28* (2), 249-275.

17. Matsumoto, H.; Mizukoshi, T.; Nitta, K.; Minagawa, M.; Tanioka, A.; Yamagata, Y., Organic/inorganic hybrid nano-microstructured coatings on insulated substrates by electrospray deposition. *Journal of colloid and interface science* **2005**, *286* (1), 414-416.
18. Lei, L.; Kovacevich, D. A.; Nitzsche, M. P.; Ryu, J.; Al-Marzoki, K.; Rodriguez, G.; Klein, L. C.; Jitianu, A.; Singer, J. P., Obtaining Thickness-Limited Electrospray Deposition for 3D Coating. *ACS applied materials & interfaces* **2018**, *10* (13), 11175-11188.
19. Kovacevich, D. A.; Lei, L.; Han, D.; Kuznetsova, C.; Kooi, S. E.; Lee, H.; Singer, J. P., Self-Limiting Electrospray Deposition for the Surface Modification of Additively Manufactured Parts. *ACS Applied Materials & Interfaces* **2020**, *12* (18), 20901-20911.
20. Lei, L.; Gamboa, A. R.; Kuznetsova, C.; Littlecreek, S.; Wang, J.; Zou, Q.; Zahn, J. D.; Singer, J. P., Self-limiting electrospray deposition on polymer templates. *Scientific Reports* **2020**, *10* (1), 17290.
21. Bodnár, E.; Rosell-Llompart, J., Growth dynamics of granular films produced by electrospray. *Journal of Colloid and Interface Science* **2013**, *407* (0), 536-545.
22. Lei, L.; Chen, S.; Nachtigal, C. J.; Moy, T. F.; Yong, X.; Singer, J. P., Homogeneous gelation leads to nanowire forests in the transition between electrospray and electrospinning. *Materials Horizons* **2020**, *7* (10), 2643-2650.
23. Kovacevich, D. A.; Lei, L.; Han, D.; Kuznetsova, C.; Kooi, S. E.; Lee, H.; Singer, J. P., Self-Limiting Electrospray Deposition for the Surface Modification of Additively-Manufactured Parts. *ACS Applied Materials & Interfaces* **2020**.
24. Nasir, M.; Matsumoto, H.; Minagawa, M.; Tanioka, A.; Danno, T.; Horibe, H., Preparation of PVDF/PMMA blend nanofibers by electrospray deposition: effects of blending ratio and humidity. *Polymer journal* **2009**, *41* (5), 402-406.
25. Pitsalidis, C.; Pappa, A.; Hunter, S.; Laskarakis, A.; Kaimakamis, T.; Payne, M.; Anthony, J.; Anthopoulos, T.; Logothetidis, S., High mobility transistors based on electrospray-printed small-molecule/polymer semiconducting blends. *Journal of Materials Chemistry C* **2016**, *4* (16), 3499-3507.
26. Liao, Y.; Fukuda, T.; Takagi, K.; Kamata, N.; Fukuda, F.; Furukawa, Y., High crystallinity parameter poly (3-hexylthiophene-2, 5-diyl) thin film fabricated by the electrospray deposition method. *Thin Solid Films* **2014**, *554*, 132-136.
27. Lei, L.; Chen, S.; Nachtigal, C.; Moy, T.; Yong, X.; Singer, J. P., Homogeneous gelation leads to nanowire forests in the transition between electrospray and electrospinning. *ChemRxiv* **2020**.
28. Varga, Á.; Brunelli, N. A.; Louie, M. W.; Giapis, K. P.; Haile, S. M., Composite nanostructured solid-acid fuel-cell electrodes via electrospray deposition. *Journal of Materials Chemistry* **2010**, *20* (30), 6309-6315.
29. Chaparro, A.; Gallardo, B.; Folgado, M.; Martín, A.; Daza, L., PEMFC electrode preparation by electrospray: optimization of catalyst load and ionomer content. *Catalysis Today* **2009**, *143* (3-4), 237-241.
30. Kovacevich, D. A.; Lei, L.; Han, D.; Kuznetsova, C.; Kooi, S. E.; Lee, H.; Singer, J. P., Self-Limiting Electrospray Deposition for the Surface Modification of Additively Manufactured Parts. *ACS Appl Mater Interfaces* **2020**, *12* (18), 20901-20911.
31. Chung, P. C.; Glynos, E.; Green, P. F., The Elastic Mechanical Response of Supported Thin Polymer Films. *Langmuir* **2014**, *30* (50), 15200-15205.
32. Bates, F. S.; Fredrickson, G. H., Block Copolymer Thermodynamics: Theory and Experiment. *Annual Review of Physical Chemistry* **1990**, *41* (1), 525-557.

33. Jeong, U.; Ryu, D. Y.; Kho, D. H.; Lee, D. H.; Kim, J. K.; Russell, T. P., Phase Behavior of Mixtures of Block Copolymer and Homopolymers in Thin Films and Bulk. *Macromolecules* **2003**, *36* (10), 3626-3634.
34. Han, C.-S., Indentation size effect in polymers. 2011; Vol. 10, pp 393-413.